Contents

1 Introduction **1**
1.1 History . . . 1
1.2 . . . 1

2 Theory **2**
2.1 Basics of ultrasound images . . . 2
2.2 Physics of ultrasound . . . 2
2.3 Reflection . . . 3
2.4 Absorption . . . 3
2.5 Scattering . . . 4
2.6 The bubble as a linear oscillator . . . 5
2.7 Non-linear behaviour . . . 6
2.8 The bubble as a non-linear oscillator . . . 7
2.9 Resolution and depth of view . . . 7
2.10 Speckle . . . 8

3 Cancer **8**
3.1 Tumor growth and properties . . . 8
3.2 Cancer treatment . . . 9
3.3 Targeted drug delivery . . . 10
3.4 Ultrasound mediated drug delivery . . . 10
3.5 Contrast agents . . . 11
3.6 Phase-shift bubbles . . . 12

4 Imaging modalities **15**
4.1 Contrast enhanced imaging . . . 15

5 Image processing **16**
5.1 Transducer . . . 16
5.2 Digitalization, amplification and time-gain compensation . . . 16
5.2.1 RF and IQ data . . . 17
5.2.2 Hilbert transform . . . 17
5.2.3 Downsampling . . . 18
5.3 Image registration . . . 18
5.3.1 Image transformations . . . 19
5.3.2 Similarity measure . . . 20
5.3.3 Regular step gradient descent . . . 21
5.3.4 Interpolation . . . 21
5.4 Background subtraction . . . 22

6 Image recording **29**
6.1 Sonazoid™ 29
6.2 Imaging setup 29
6.2.1 Imaging modes 29
6.3 The animals/cancer 30
6.4 Counting 16 animals 30

7 Image processing **30**
7.1 Image registration 30
7.2 Background subtraction 30
7.3 Counting 30

8 Qualitative validation **31**

9 Quantitative validation **31**
9.1 Synthesized data set 31
9.2 Phase-shift bubbles intensity distribution 32

A Derivation of the Rayleigh-Plesset equation **38**

2 Theory

2.1 Basics of ultrasound images

The basis of ultrasound imaging is the reflection of ultrasound at tissue boundaries within the body. Ultrasound is sound waves generated by a transducer, and as the wave travels through the body, echoes are generated by partial reflection at every boundary. The amount of reflection depends on the relative change in acoustic impedance at the boundary. The echo is recorded by the transducer, and it is then displayed in the image according its spatial origin. The speed of sound is approximately $1540\,\mathrm{m\,s^{-1}}$ for all soft body tissue, and it is thus easy to calculate the origin by measuring the time of travel of the echo.

2.2 Physics of ultrasound

Ultrasound is sound waves with frequency above 20 kHz, which is the upper limit of audible sound. For the purpose of medical imaging, frequencies between 1 MHz and 18 MHz are common. Sound waves are pressure waves, and the pressure fluctuations cause temporal displacement of the medium in which the wave is traveling. For most purposes the displacement is along the direction of travel, this is know as longitudinal waves. Solids can support transverse sound waves, but that is outside the scope of this thesis. The wavelength , λ, is determined by the frequency of the source and the phase velocity in the medium, c, i.e. $\lambda = \frac{c}{f}$. The phase velocity c is given by

$$c = \sqrt{\frac{1}{\rho\kappa}}, \tag{1}$$

where ρ and κ are the tissue density and compressibility. For soft human tissue the phase velocity is about $1540\,\mathrm{m\,s^{-1}}$.The compressibility is a measure of the relative change in volume from change in pressure, that is $\kappa = -\frac{1}{V}\frac{\partial V}{\partial p}$. Here V is volume and p pressure.

The propagation of a sound wave traveling in the x-direction can in a fluid be described by the wave equation, i.e.

$$\frac{\partial^2 W}{\partial x^2} = \frac{\rho_0}{G}\frac{\partial^2 W}{\partial t^2}. \tag{2}$$

Here W is the particle displacement, ρ_0 the density of the medium and G the bulk modulus. The bulk modulus is the reciprocal of the compressibility, and is a measure of the volume stiffness. A general solution to this equation is

$$W = W_0 \exp^{i(kx-\omega t)}, \tag{3}$$

where ω is the angular frequency, $k = \frac{\omega}{c}$ the wave number, and c the phase velocity as given in Equation (1), with κ substituted by $\frac{1}{G}$. The pressure variations is then given by particle velocity $u_x = \frac{\partial W}{\partial t}$ as

$$p_z = \rho_0 c u_x. \tag{4}$$

It is important to emphasize the difference between the phase velocity and the particle velocity. The phase velocity is the velocity of energy carried through the medium, while the particle velocity is the velocity of the local displacement of particles.

The acoustic impedance Z of the medium is defined as the ratio of the pressure to the particle velocity,

$$Z = \frac{p_x}{u_x} = \rho c. \tag{5}$$

2.3 Reflection

Reflection provide the basis for ultrasound imaging, and occurs when the wave encounter a planar surface with a change in acoustic impedance. Across this surface both the pressure and particle velocity have to be continuous. From these boundary conditions the intensity coefficients of the reflected r_i and transmitted t_i wave can be given as [25]

$$r_i = \left(\frac{z_2 \cos\theta_i - z_1 \cos\theta_t}{z_1 \cos\theta_t + z_2 \cos\theta_i} \right)^2 \tag{6}$$

$$t_i = \frac{4 z_2 z_1 \cos^2\theta_i}{(z_2 \cos\theta_i + z_1 \cos\theta_t)^2}. \tag{7}$$

Here z_1 and z_2 are the acoustic impedance in medium 1 and 2, shown in Figure ?????. The angle of reflection θ_r is equal the angle of incidence θ_i, while the angle of transmission θ_t is given by Snell's law [1], $c_2 \sin\theta_i = c_1 \sin\theta_t$.

2.4 Absorption

Loss of kinetic energy to heat from the propagating wave to the surrounding medium is known as absorption. Absorption occur continuously and reduce the amplitude of the wave. For linear propagation of a pressure wave, this can be described as

$$p(x) = p(0) \exp^{-\alpha_A(\omega)x}, \tag{8}$$

where $p(0)$ is the initial pressure amplitude, $alpha_A$ the absorption coefficient and ω the angular frequency.

For non-linear propagation the absorption depends on the local amplitude, and in the diagnostic intensity range the non-linear interaction is proportional to the square of the intensity [2]. Non-linear propagation also affects the shape and frequency spectrum of the propagating wave, and can usually not be ignored for contrast agent applications [8].

2.5 Scattering

Scattering is reflection that occur when the size d of the surface encountered is comparable or smaller than the wavelength. Scattering can arise from inhomogenities in compressibility or density. Scattering reflects the wave in a large range of directions, and the backscattered signal received at the transducer is therefore weak compared to reflected echoes. The magnitude and direction of the scattering depends on the size of the scatterer and increase strongly with the frequency.

If we consider an incoming plane wave propagating in the direction *hati*, see Figure **??**, the incident pressure, p_i, at the scatter located at $\mathbf{r}_0$ is then

$$p_i(\mathbf{r}_0, t) = p_0 \exp^{i(\mathbf{r}_0 \mathbf{k}_i - \omega t)}. \tag{9}$$

If we only consider the far field the scattered wave, p_s, at the observer at $\mathbf{r}$ is given by [8]

$$p_s(\mathbf{r}, t) = f(\hat{r}, \hat{i}) \frac{\exp^{ik_s(\mathbf{r}-\mathbf{r}_0}}{|*|\,\mathbf{r} - \mathbf{r}_0} p_i(\mathbf{r}_0, t). \tag{10}$$

The $f(\hat{r}, \hat{i})$ is the scattering amplitude function. The scattered intensity is

$$I_s = \frac{1}{2}\frac{|*|\,{p_s}^2}{\rho c} = \frac{1}{2}\frac{|*|\,{p_i}^2}{\rho c}\frac{|*|\,f(\hat{r}, \hat{i})^2}{|*|\,{\mathbf{r} - \mathbf{r}_0}^2} = I_i \frac{|*|\,f(\hat{r}, \hat{i})^2}{|*|\,{\mathbf{r} - \mathbf{r}_0}^2}, \tag{11}$$

where I_i is the incident intensity. The differential scattering cross-section is defined as $\sigma_d = |f(\hat{r}, \hat{i})|^2$. The scattering cross section is the integral of the differential cross section over all solid angles, i.e.

$$\sigma_s = \int_{4\pi} \sigma_d \mathrm{d}\Omega. \tag{12}$$

The Rayleigh scattering model is the simplest model for scattering of small particles, i.e. particles with a diameter $d << \lambda$. This model do not take damping or resonance effects into account. If we again consider the plane wave, the differential scattering cross section is given by [**?**]

$$\sigma_d = k^4 a^6 |*| \left(\frac{G - G_0}{3G} - \frac{\rho - \rho_0}{2\rho + \rho_0} \cos\theta \right)^2. \tag{13}$$

The total cross-section is obtained using Equation (12) and (13),

$$\sigma_s = 4\pi k^4 a^6 \left[\left(\frac{G - G_0}{3G} \right)^2 + \frac{1}{3} \left(\frac{\rho - \rho_0}{2\rho + \rho_0} \right)^2 \right]. \tag{14}$$

In these equations k is the wavenumber, a the radius of the scatterer, and the zero subscript refer to properties of the surrounding medium. The angle θ is the angle between the incident wave and the scattered wave, i.e. $\theta = 180\,\text{deg}$ is the direction of backscatterering. Although these equations represent a coarse approximation, it demonstrates why gas bubbles are excellent contrast agents. The density term in Equation (14) is limited to $1/3$, while the bulk modulus term has no upper limit as G gets small compared to G_0. Thus, it is the compressibility and not the acoustic impedance which is the main cause to the scattering off a gas bubble. This is shown in Figure

It is important to keep in mind that it is the backscattering and not the total scattering which determines the received signal, and Equation (13) give therefore a more correct image than Equation (14).

2.6 The bubble as a linear oscillator

The following section follows the derivation of the bubble as a linear oscillator in [**?**], which contains a full review of the subject acoustic properties of contrast agents. To include the effects of damping and resonance, the microbubble can be modeled as a harmonic oscillator. Comparing the bubble with a mass/spring system, Figure **??**, the gas pressure, surrounding liquid and radiation resistance corresponds to the spring, mass and dash-pot, respectively. The limitation for linear oscillations is that the radial displacement of the bubble wall is small compared to the bubble radii.

As the bubble oscillates both the gas inside and the liquid outside the bubble add inertia to the system. Due to the relative low density of the gas, this contribution can be neglected. The gas inside the bubble act against any volume change of the bubble, thus acting as the spring in the system. The damping of the system is caused by heat transport to the surroundings, radiation of sound and by the viscosity of the liquid. If we consider a bubble with a shell, viscous forces in the shell contributes to the damping.

For this system the resonance frequency f_0 is given as [**?**]

$$f_0 = \frac{\omega}{2\pi} = \frac{1}{2\pi a} \sqrt{\frac{3\kappa p_0}{\rho} + \frac{12 G_s d_s}{a}}. \tag{15}$$

Here a is the bubble radius, G_s and d_s the shear modulus and thickness of the shell, p_0 the atmospheric pressure and κ the polytropic exponent pf the gas.

The polytropic exponent is equal the adiabatic constant γ for if the oscillations are adiabatic, while it is one for isothermal conditions. This depends on the bubble radius and signal frequency [**?**]. The second term on the right-hand side of Equation (15) is the contribution from the shell to the bulk modulus of the system.

The scattering cross section is

$$\sigma_S = 4\pi a^2 \frac{\Omega^4}{(1-\Omega^2)^2 + (\Omega\delta)^2}, \tag{16}$$

where $\Omega = {}^{\omega}/_{\omega_0}$ and δ the damping constant of the system.

The scattering cross section for air bubbles and Sonazoid™are plotted in Figure **??**. We see that the presence of a shell increase the resonance frequency and broadens the resonance peak [8].

2.7 Non-linear behaviour

Til now we have only considered the linear behavior for both the wave propagation and the bubble scattering and oscillation. A brief review of non-linear wave propagation follows, before a section on the bubble as a non-linear oscillator. A full review of these subjects are found in [**?**] and [**?**].

When the amplitude of the acoustic wave exceeds about 1 MPa non-linear propagation become noticeable [**?**]. Non-linear effects can be divided into local and cumulative. Local effects are displacement of vibrating sources, and differences in the relationship between pressure and particle velocity. Local effects are regarded as negligible, except for oscillating microbubbles where there is a change the pressure/bubble radius relationship [**?**].

Cumulative effects are caused by differences in the propagation speed at different locations in the wave. At the peak pressure the tissue will be compressed, increasing the speed of sound. In the region of rarefaction the propagation speed is decreased. This cause distortion of the waveform which will develop with distance, see Figure **??**. The compression peak will move in the direction of propagation, while the rarefaction peak move in the opposite direction. This will decrease the distance between the two peaks, til they are coincident and we get a discontinuity of the wave.

The distortion of the waveform generates high frequency components in the pulse frequency spectrum. These high frequency components appear at multiples of the fundamental frequency f_0, and are called harmonic frequencies. This is seen in Figure **??**. As the wave propagates further the high frequencies are more attenuated, and the wave will eventually regain its shape with a reduced amplitude.

2.8 The bubble as a non-linear oscillator

The non-linear response from a microbubble is in general not negligible. It is actually the property of interest, when used as contrast agents in diagnostic imaging, see Section 4.1. A brief review of the non-linearity of bubble oscillations is given below. A full review is outside the scope of this thesis, and the interested reader is addressed to [**?**].

Compared to tissue, the non-linear response from microbubbles are large, and further increased by the coincidence of the resonance frequency being in the range of frequencies used in diagnostic imaging. The non-linear response from the contrast agent Optison™is seen in Figure **??**. The presence of harmonic peaks proves the non-linear response of the microbubble.

The non-linear dynamics of a spherical bubble in a infinite, incompressible fluid can be described by the Rayleig-Plesset equation,

$$\frac{p_{R_0}\left(\frac{R_0}{R}\right)^{3\gamma} - p_0 - p(t)}{\rho_l} = \frac{3\dot{R}^2}{2} + R\ddot{R}, \tag{17}$$

where $R = R(t)$ is the bubble radius as a function of time, and $\dot{R}$ and $\ddot{R}$ the velocity and acceleration of the bubble wall, respectively. FIX beskrivelse a ligning!!!!.

This is an ordinary differential equation which can be solved with initial conditions $R(0) = R_0$, and $\dot{R} = 0$ [18]. IINSERT FIGURES from ANDY???

2.9 Resolution and depth of view

The ultrasound waves used in medical imaging are emitted as short pulses, where the pulse length determines the longitudinal resolution. It is not possible to distinguish two points in the longitudinal direction separated by a distance shorter than half the pulse length. A short pulse is therefore desirable in order to produce good longitudinal resolution. The theoretical minimum pulse length is one wavelength, although this is difficult to achieve in practice, and a few wavelengths is a more realistic minimum. A short pulse will contain a wider band of frequencies than a long pulse.

The required depth of view will depend on how deep the tissue subject to the imaging is located, but there will always be a finite required depth penetration. The attenuation of ultrasound is proportional to the frequency, so a good depth of view implies a low frequency. Hence, there will always be a trade off between good longitudinal resolution and depth of view, and the diagnostic frequency will be chosen according to the patient and application.

Lateral resolution is the minimum distance perpendicular to direction of propagation required to distinguish two objects. This is determined by the width of the

beam, and may vary with the depth of view. It is common to focus the beam to obtain the best resolution at the depth of interest. Strong focusing will give very good resolution at a very limited depth range, while weak focusing give medium resolution through most of the image. Temporal resolution is determined by the frame rate, which is typically between 10 and 30 frames per second.

2.10 Speckle

Speckle is a random, deterministic speckle pattern present in all types of coherent imaging, thus also in ultrasound images. The speckle is formed by scatterers smaller than the resolution of the imaging system, and the shape and size of the speckle pattern is determined by the dimensions of the imaging system and the structure of the imaged tissue.

The speckle is an interference phenomenon created by coherent waves with different phase and amplitude added together. If several echo waves arrive at the same piezoelectric element within a time span shorter than the emitted pulse, the piezoelectric element will not be able to distinguish the waves, and their impact will be added.

3 Cancer

3.1 Tumor growth and properties

A tumor is a mass of tissue with abnormal growth, and may either be benign or malignant. A benign tumor is localized with a well-defined boundary and do usually not pose any health threat. A malignant tumor is what we know as cancer, and can invade adjacent tissue, perform metastasis and be life threatening.

A cancer starts off from one abnormal cell, which proliferates through cell division resulting in uncontrolled growth. To maintain growth beyond a critical size of about 1 mm [12], new blood vessels are induced through angiogenesis to meet the need of nutrients and oxygen.

The cell growth is regulated by two types of genes. Proto-oncogenes regulate normal cell proliferation, while the tumour suppressor genes control repair of cell damage, cell death and growth inhibition. Mutation or loss of any of these regulatory systems can cause cancer growth.

The invasion of adjacent, normal tissue distinguish the malignant tumour from the benign, and this happens along along the pathways of least resistance, i.e. along vessels or fascia. This invasion is enhanced by increased amount of proteases outside the tumor boundary, which increase mobility of the cancerous cells. This

also enhance the metastasis, where the cancer is spread along the lymphatic vessels, blood vessels or the peritoneal cavity to a new site.

An important feature which cause the possibility of localized drug delivery, is the structure of the cancer vasculature. This vasculature is developed through the angiogenesis, which is enhanced by Vascular endothelial growth factors(VEGFs). The VEGFs diffuse through the extracellular matrix(ECM) and connect to receptors on the inner surface of the vessel walls(Endothelial cells) [14]. This stimulate both the production of more endothelial cells and the construction of new vessels through the extracellular matrix [19]. This results in a structure which differ from normal vasculature. The tumour vasculature has increased vessel density and vessel size, a large amount of dead-ends and a disordered branching pattern.

The abnormal level of endothelial cells leads to vascular walls which lack in coverage of perivascular cells and tight adherens junctions which stabilize the vessel. Hence, there will be large intracellular spaces in the vessel wall, and the vessel becomes leaky. This allow the cancer cells to enter the vasculature, enhance macromolecular transport through the vessel wall, and increase interstitial pressure within the tumour. This is known as the *enhanced permeability and retention*(EPR) effect. The EPR effect leads to accumulation of macromolecules within the tumour, and enhance local delivery of cancer drugs.

3.2 Cancer treatment

Despite the massive amount of research on the field of cancer, all existing treatments suffer from side-effects and limited results. Most types of cancer are strongly related to lifestyle. Prevention is therefore the most important action in the battle against cancer. Another important action is screening, which can reveal cancer in an early stage. Early detection has shown to be decisive for the outcome of the cancer treatment [12] [11].

The current treatments can be divided into chemotherapy, radiotherapy or surgery. Surgery aim to remove the entire tumour and, if possible, any metastases in regional lymphatics. Surgeries may be difficult to perform without damaging adjacent tissue. Radiotherapy is performed by radiating the tumour with high-energy X-rays to kill the malignant cells by causing fatal damage to their DNA. Some healthy tissue such as the lens at end of the spinal cord are very vulnerable to radiation, and can be damaged it exposed to a high radiation dose. Both of these treatments are best suited for not-metasized tumours.

Chemotherapy use cytotoxic or cytostatic drugs to kill malignant cells or prevent further growth. The drugs are distributed through the circulatory system, and only a small fraction of the dose reach the malignant cells. The rest of the dose cause dangerous side effects to healthy tissue [20]. These side effects limits the dose to a low level. This is described by a very low therapeutic index, which

is the ratio between the maximum tolerated dose, and the minimum dose required for any therapeutic effect.

3.3 Targeted drug delivery

Increased targeting of the chemotherapeutic drugs enables the delivery more drug to the malignant cells without increase in the total dose. The increased leakiness of the tumour vasculature and the over-expression of specific receptors, are two of the characteristic properties of tumour tissue which provide possibilities for targeted delivery. Recent research has enabled drug carriers on nanoscale which utilize these possibilities [10]. The research in this field can be divided into passive, active and triggered targeting.

Passive targeting relies on the accumulation of drug in cancerous tissue due to the EPR effect. The drug is loaded into drug carriers which are only able to penetrate the endothelial layer if the EPR efeect is present [**?**]. The carriers are designed to remain in the circulatory system for a long time to provide sufficient accumulation in the tumour. These carriers are of a size 10 nm to 500 nm, although the lower cut off size varies [**?**]. This targeting is limited by the vascularity and leakiness of the tumour, and the slow diffusion present in large tumours.

Active targeting is carried out by drug carriers where the surface is capable of recognition and binding to a target site in the tumour vasculature. This is shown in Figure ?. Triggered targeting use drug carries sensitive to exposure of ultrasound or to the changes in pH or enzymes which occur in cancerous tissue. Ultrasound mediated drug delivery is addressed below.

3.4 Ultrasound mediated drug delivery

Ultrasound is an attractive trigger for targeted drug delivery as it is non-invasive, generally safe and well characterized. It is proved that ultrasound enhance the cell membrane permeability, in particular if microbubbles are present [**?**]. This is known as sonoporation. The proposed model is that the microbubbles enhance the EPR effect because of the oscillation initiated by the ultrasound, see Figure **??**. The oscillation moves the cell membrane and create hydrophilic pores which enables transport of fluid or macromulecules through the membrane [**?**].

There are several strategies for using sonoporation to enhance drug delivery. Small amounts of hydrophilic drug can be attached to the surface of the microbubble, or hydrophobic drug can be incorporated into the shell of the microbubble. The drug is then released as the microbubbles are disrupted by an ultrasound pulse [**?**]. Drug has also been loaded into liposomes and administered together with microbubbles, but the effect is then very dependent of the simultaneous localization of the liposome and microbubble in the tumour vasculature. To ensure

the co-localization the microbubble and the drug can be encapsulated together within a liposome membrane shell [**?**].

3.5 Contrast agents

Contrast agents are used to increase the image sensitivity and signal-to-noise ratio in medical imaging. In ultrasound imaging, this is accomplished by intravenous injection of a solution containing gas-filled microbubbles. Microdroplets are also used [21], but in much less extent than gas bubbles and is outside the scope of this thesis. Microbubbles are favourable because of the higher echogenicity [22].

The microbubbles have to fulfill several requirements to perform as a contrast agent. The contrast agent has to be delivered to the area of interest, and this set reguirements to lifetime and size. The diameter has to be smaller than 8 µm to pass the pulmonary capillary [23], which is the size limiting factor in the circulatory system. Strong backscattering of ultrasound is important. Absorption is an unwanted effect as it attenuates the ultrasound wave without contributing to the received signal. It is also important that the contrast agent is well tolerated by the body and is able to leave the circulatory system either by dissolving or by being phagocytosed by the kupfer cells in the liver [8].

The first contrast agents were made by saline, and was put to use by cardiologists in the 1960s for identification of mitral valve echoes. The saline was shaken before injection to create the microbubbles. Current available contrast agents have been able to fulfill the requirements stated, and consist of a gas enclosed in a suited shell. The shell has to be biocompatible and is made from fat, proteins or polymers. The advantage of a shell is increased lifetime and scattering of ultrasound. The size of the microbubbles is approximately equal to the size of red blood cells, i.e. (2 µm to 6 µm).

The microbubbles have two important properties which cause large scattering. The first reason is the big difference in acoustic impedance between microbubbles and blood. The second property is the compressability of the gas inside the microbubble. The pressure fluctuations caused by the ultrasound forces the microbubble to expand during rarefaction and contract during compression. The microbubble will oscillate with the same frequency as the ultrasound source, and the scattering will be strongest at the resonance frequency of the microbubble. The resonant frequency is determined by the properties and the size of the shell.

The use of contrast agents has been limited to diagnostics, but these microbubbles possess properties suited therapeutic use. The microbubbles can serve as carriers for ultrasound mediated drug delivery [4], see section ?????.

3.6 Phase-shift bubbles

The drug carrier used in this project is a two component particle composed of negatively charged gas microbubbles and positively charged droplets, known as Acoustic cluster therapy (ACT). Both the gas microbubble and the droplet have an initial size about 2 µm to 3 µm. The gas microbubble consist of a low solubility perfluorocarbon gas encapsulated in a negatively charged phospholipid membrane, e.g. Sonazoid™. The drug is dissolved in a perfluorated oil phase and stabilized by a positively charged phospholipid membrane. When the bubbles and droplets are mixed, clusters of droplets and bubbles will form due to electrostatic attractive forces.

When the clusters are exposed to ultrasound of standard medical frequency(2 MHz to 15 MHz [**?**]) and intensity,the microbubble will oscillate and transfer energy to the droplet through mechanical interactions at the boundary. This initiate a fusion into a gas and liquid mixture, encapsulated by a mixed surfactant membrane. The fluid will vaporize and expand to a gas bubble of approximately 30 µm. The enlarged gas bubble can block the capillary network and maintain the local concentration of the released drug.

If we assume rapid thermal conduction from surrounding blood, the partial pressure of pf-MCP will be close to the vapour pressure at body temperature. This vapour pressure is lower than the local hydrostatic pressure, and the difference is initially equalized by the gas from the microbubble. An inward diffusion of $O_2, N_2, CO_2, H_2OandAr$ will exist simultaneously, and these gases will also contribute to the equalization of the hydrostatic pressure. The inward diffusion is driven by partial pressure gradients of the respective gases.

The evaporation will not occur if the blood is under-saturated of the aforementioned gases. If the hydrostatic pressure inside the bubble is too large, there will be no pressure gradient to drive the inward diffusion. This is caused by too high surface tension or hydrostatic pressure in the surrounding blood, and this stop the evaporation. This initial evaporation occurs in a second or less [7]. The inward diffusion may continue after the evaporation, until a maximum size is reached after approximately 20-30 seconds(Ref?).

Application of low MI and low frequency(0.1 MHz to 2 MHz ultrasound will drive an oscillation of the large phase-shift bubbles and increase the permeability of the adjacent vasculature(REF?). This allow diffusion of the drug through the vessel walls to the cancer cells. The increased permeability will cease when the ultrasound is turned off leaving the drug trapped within the tumour.

A more mathematical description of the aforementioned evaporation is given now [7]. We assume we can use the simplification that the gases are ideal gases, i.e. we can use the ideal gas law

$$PV = nRT. \tag{18}$$

Hence, the volume of evaporated gas, v_{pf}, is a function of the initial volume and pressure in the oil droplet, i.e.

$$V_g(V_{pf}, p_{pf}) = \frac{n_{pf}RT}{p_{pf}} = \frac{V_{pf}\rho_{pf}RT}{M_{pf}p_{pf}}. \tag{19}$$

We assume the body temperature T to be 310 K. If also assume that both the gas and liquid bubble are spherical, we have the simple relation between diameter and volume, $V = \frac{\pi d}{6}$, and using this and Equation (19), we get an expression for the diameter of the gas bubble,

$$d_g(p_{pf}, d_{pf}) = d_{pf}\sqrt[3]{\frac{\rho_{pf}Rt}{M_{pf}p_{pf}}}. \tag{20}$$

From this equation we can get the size of the gas bubble after the initial evaporation. For an initial diameter of 4 µm we get a diameter about 23.4 µm, knowing that the vapour pressure of pf-MCP at body temperature is 76 kPa [7]. To include surface tension we use the Young-Laplace equation for a sphere,

$$\Delta p = \gamma\frac{4}{d}, \tag{21}$$

to get an expression for the pressure in the surrounding fluid,

$$p_w = p_{partial} + p_{pf} - \gamma frac4d_g(p_{pf},d_{pf}). \tag{22}$$

Here p_w is the total pressure in the surrounding fluid, while p_{pf} is the partial pressure from the gases in the surrounding fluid. Combining equations above we get a cubic expression for the gas bubble diameter,

$$(p_w - p_{partial})D_g^3 + 4\gamma D_g^2 - \frac{6v_{pf}\rho_{pf}RT}{\pi M_p f}. \tag{23}$$

This equation has a real solution, and can be used to calculate an upper limit for the phase-shift gas bubble diameter. This is shown in Figure ???.

In addition to the static description above, we can derive an expression for the dynamic bubble growth. The following is a simplified model.

There exist a mechanical equilibrium(pressure) at the bubble boundary, and from the ideal gas law (Equation (18)) we have that

$$p_A + p_{pf} = \frac{2\gamma}{r} + p_{atm} + p_{blood}, \tag{24}$$

where

$$p_A + P_{pf} = (C_A + C_{pf})RT. \tag{25}$$

Using both Fick's first law of diffusion and that a change in mass have to cause a flux through the boundary ($J = -\frac{\mathrm{d}n}{\mathrm{d}t}$), we have that

$$J_{pf} = -\frac{\mathrm{d}}{\mathrm{d}t}\left(\frac{4\pi C_{pf} r^3}{3}\right) = 4\pi r(c_{pf}(r) - c_{pf}(\infty)), \tag{26}$$

and a similar expression for J_A. Note that the diffusion flux J is given in mol per second. We can assume that the concentration of pf-MCP goes to zero for far from the bubble, i.e. $c_{pf}(\infty) = 0$. We get two differential equations,

$$-\frac{\mathrm{d}}{\mathrm{d}t}(C_{pf} r^3) = 3rD_{pf}L_{pf}C_{pf}, \text{and} -\frac{\mathrm{d}}{\mathrm{d}t}(C_A r^3) = 3rD_A L_A\left(C_A - \frac{p_{air}}{RT}\right). \tag{27}$$

Here L is the concentration Ostwald coefficient describing the solubility of a gas, $L = \left(\frac{c}{C}\right)_{equilibrium}$ [5]. Lower-case c_x is the concentration x in the liquid phase, while upper-case C_x is the concentration of x in the vapour phase. Under saturation of air is incorporated in the term $\frac{p_{air}}{RT}$.

We rewrite the these equations with dimensionless variables to get

$$F + A = \mu\rho^2 + (1+\vartheta)\rho^3, \quad \frac{\mathrm{d}F}{\mathrm{d}\Gamma} = -\frac{3L_{pf}}{\rho^2}F \quad \text{and} \quad \frac{\mathrm{d}A}{\mathrm{d}\Gamma} = -\frac{3\delta L_A}{\rho^2}(A - p_d\rho^3), \tag{28}$$

with the dimensionless variables

$$\mu = \frac{2\gamma}{p_{atm}r_0}, \quad \vartheta = \frac{p_{blood}}{p_{atm}}, \quad \rho = \frac{r}{r_0}, \quad \chi_A = \frac{C_A RT}{p_{atm}},$$
$$\chi_{pf} = \frac{C_{pf}RT}{p_{atm}}, \quad \Gamma = \frac{D_{pf}}{r_0^2}t, \quad A = \chi_A\rho^3, \quad F = \chi_{pf}\rho^3, \quad \text{and} \quad p_d = \frac{p_{air}}{p_{atm}}. \tag{29}$$

Combining equations we get a differential equation for ρ,

$$\frac{\mathrm{d}\rho}{\mathrm{d}\Gamma} = \frac{-3\delta L_A(A - p_d\rho^3) - 3L_{pf}(\mu\rho^2 + (1+\vartheta)\rho^3 - A)}{\rho^3(2\mu + 3(1+\vartheta)^r ho)}. \tag{30}$$

These three differential equations can be solved using appropriate initial conditions. Defining the variable X_{pf} to be the initial mole fraction of pf-MCP, we get the initial conditions

$$F(0) = X_{pf}(\mu + \vartheta + 1), \quad A(0) = (1 - X_{pf})(\mu + \vartheta + 1) \quad \text{and} \quad \rho(0) = 1. \tag{31}$$

The growth of the bubble radius and volume is calculated from these differential equations and shown in Figure ???.

4 Imaging modalities

Ultrasound images of can be captured using several different modalities to enhance different properties of the tissue. The simplest modality is the amplitude-mode(A-mode), where a single element transducer scans is used to generate echoes along one line, and the received echoes are plotted as a function of depth. Brightness-mode(B-mode) use an array of transducers to generate 2D map of a slice through the body, where the image brightness is proportional to the echo originated from the corresponding location. Motion mode (M-mode) is generated from a sequence of A- or B-mode images to image tissue motion. Doppler imaging is another large field of imaging mode, where the Doppler effect is utilized to image the blood flow. This can used to measure the velocity, direction and total blood flow.

4.1 Contrast enhanced imaging

Due to the non-linear behavior of the microbubbles in contrast agent, non-linear techniques are often applied to enhance the contrast-to-tissue signal ratio. Non-linear imaging techniques can divided into hi- and low-MI. For high-MI images the acoustic pressure is large enough to destroy most of the microbubbles in the imaging plane, releasing free gas bubbles and crating a short flash of high contrast. In low-MI images (MI 0.05) to 0.1) few of the bubbles are disrupted and the non-linear scattering properties are used to form images. Different low-MI techniques are described below.

Second harmonic imaging is based on a transducer with a bandwidth covering both the fundamental transmit frequency, and its second harmonic, see Figure **??**. Even at moderate pressure (0.1 MPa to 0.3 MPa) microbubbles generate harmonic frequencies, and by excluding the fundamental frequency from the received signal, only the non-linear signal is recorded, and this increases the contrast-to-tissue ratio. The required bandwidth of the transducer give limitations to the spatial resolution.

Phase inversion is another non-linear mode used to image contrast agents. Two pulses are emitted from the transducer, where the second pulse is 180° out of phase with the first pulse, see Figure **??**. When the two received signals are added, the linear part sum to zero because of the linear response to the applied pressure. The microbubbles are the principal source of the non-linear part in the image, and they will therefore be emphasized by this technique.

Amplitude modulation is another technique used to enhance the contrast-to-tissue ratio. Two or three pulses are emitted with different amplitudes. The tissue will respond linearly to the amplitude, while the non-linear response from the microbubbles increase dramatically to the increased amplitude. The linear response can be removed by subtracting the received signals. A combination of

the phase-inversion and the amplitude modulation is also possible.

5 Image processing

5.1 Transducer

A transducer has the capability to transform applied electrical signals to pressure waves and vice versa. It is therefore responsible for both emitting ultrasound pulses and receiving echoes in an ultrasound apparatus. A good transducer perform this task with high conversion efficiency and without introduction of noise.

The key element of the transducer is the piezo-electric element, which is a shaped piece of either a piezoelectric ceramic (lead zirconate titanate, PZT) or plastic (polyvinylidine difluoride, PVDF) coated with silver electrodes on the front- and backside. A voltage across the electrodes correspond to a proportional change of the thickness of the piezo-electric element.

The speed of sound, c, in a piezo-electric element is approximately $4000\,\mathrm{m\,s^{-1}}$. The fundamental resonance is at $\lambda/2$, so the thickness, T, is given by the choice of the frequency f, i.e.

$$T = \frac{\lambda}{2} = \frac{c}{2f} = \frac{2}{f(\mathrm{Mhz})}. \tag{32}$$

Hence, the frequency range of a transducer i limited to a band around the fundamental resonance, and is determined by the thickness of the piezo-electric element.

The front of the piezo-electric element is covered by a matching layer which increase the efficiency be reducing the difference in acoustic impedance between the element and the tissue. The back is covered by a backing medium which give mechanical support, provide mechanical damping.

Today's transducers usually have an array of piezo-electric elements. The advantage is the possibility of beam steering, translation and focusing, and enables parallel processing which can reduce acquisition time, speckle and signal-to-noise ratio(SNR) [6].

5.2 Digitalization, amplification and time-gain compensation

After the echoes have reached the transducer a signal is produced by making an image with the brightness at each pixel determined by the strength of the echo from that corresponding distance and direction. The first step in the image processing is to convert the signal from analogue to digital. The digital signal is less vulnerable to noise and distortion, and it enables further digital image processing. Then

a linear amplifier apply the same amount of gain to the entire signal, to make the signal strong enough for further processing. Time-gain compensation is then applied to make echoes from similar interfaces equal, regardless of the depth of their origin. This is performed by increasing the gain with increasing depth of echo. The depth of the echo is identified by the arrival time at the transducer. The rate of attenuation of ultrasound with depth is determined by the frequency and tissue.

After amplification and time-gain compensation the dynamic range of the signal is about 60 dB. The dynamic range of a signal is defined as the ratio between the largest amplitude that can be recorded without causing distortion and the lowest amplitude that can be distinguished from noise. The dynamic range of a common screen is about 20 dB. The signal must therefore be compressed before it can be displayed. To compress the dynamic range from 60 to 20 dB, an amplifier with non-linear gain is applied. Low amplitudes are amplified more than high, and the dynamic range is therefore decreased. Compression allows weak echoes from scattering within tissue to be displayed together with strong echoes from tissue interfaces.

5.2.1 RF and IQ data

RF is short term for radio frequency data which is used in ultrasound as a description for unprocessed data. IQ is short term for in quadrature, and refers to a demodulation of the RF signal to reduce the amount of storage space without loss of information. IQ modulation converts the signal from the real to the imaginary space. The IQ signal is obtained using a IQ-demodulator to down-mix, low-pass filter and decimate the RF signal. The IQ signal can be computed through a Hilbert transform [13].

5.2.2 Hilbert transform

The Hilbert transform is a linear operator which acts on a signal $u(t)$ to derive an analytic signal. The Hilbert transform convert the signal from real to complex space by adding or subtracting 90 degrees. It is therefore also known as a phase-shift operator. An analytic signal has by definition only positive frequencies in its Fourier transform, and is related to the Hilbert transform through

$$\tilde{x}(t) = x(t) + x_h(t), \tag{33}$$

where $x(t)$ is the signal, $x_h(t)$ the Hilbert transform of the signal, and $\tilde{x}(t)$ the analytic signal. The Hilbert transform can be written as a convolution,

$$x_h(t) = x(t) * \frac{1}{\pi t}, \tag{34}$$

which can be interpreted as a filtering operation with a quadrature filter which shifts all sinusoidal components by a phase shift of $\frac{\pi}{2}$. The envelope is the amplitude of the analytic signal, and a B-mode image is created from the envelope of the signal.

5.2.3 Downsampling

Because it is the envelope that is used to create the B-mode images, further reduction in data size can be achieved by downsampling of the RF signal. The RF signal is downsampled by a decimation factor M, by only recording every Mth sample.

The RF signal is a strictly bandlimited signal, limited by the bandwidth of the transducer. The envelope is thus also a bandlimited signal, with a finite maximum frequency. According to the Nyquist-Shannon sampling theorem, this signal can be sampled without aliasing or loss of information by a sampling rate twice the maximum frequency. Hence, the decimation factor, M, is determined so that

$$\frac{Fs_{RF}}{M} > 2f_{envelope}^{max}, \tag{35}$$

where Fs_{RF} is the sampling frequency of the RF signal, and $f_{envelope}^{max}$ is the maximum frequency of the envelope. For a thorough explanation, see [3].

5.3 Image registration

Image registration is the process where one image is spatially aligned to a reference image. The image to be aligned is called the moving image, while the reference image is called the fixed image. Image registration is an important part of image processing and can both be used to remove motion artifacts or to fuse images of the same object, captured with different image modalities or from different directions.

Image registration can initially be divided into extrinsic and intrinsic methods. Extrinsic methods are based on foreign objects placed into the scene before the image is captured. This has the advantage of simple, feature-based registration, but the preplacement and removal of these objects may not be trivial.

Intrinsic methods can be divided into feature and intensity based registration. Features can either be easily recognizable points identified by the user, or structures which can be extracted from the image by image segmentation. These methods are mostly used in rigid transformations, and have the advantage of being simple computations once the features are determined. One drawback is that the registration often is limited by the reliability of the segmentation or identification of the features. Although these methods are applicable to both multi-

and monomodal registration, and to different body parts, their use have in general been limited to neuroimaging and orthopedic imaging [17].

Intensity based registration differs from the other methods by using the intensity pixel values directly to compare the fixed and moving image. To compare the images a suited similarity measure is used, see section5.3.2. Using different similarity measures, this method is suitable for both multi- and monomodal registration. The image registration is then performed using an optimization routine to find the spatial translation of the moving image which minimizes the chosen similarity measure. Choosing the right similarity measure and optimization scheme is essential to get a satisfying result. For a full review of this topic, see [17].

5.3.1 Image transformations

Transformation of an image is the basis for image registration, and can be described as a mapping of a coordinate vector $\vec{x}$ from the space X to a new coordinate vector $\vec{y}$ in the space Y. The transformation is performed by a transformation matrix A, i.e. $\vec{y} = A\vec{x}$.

In 2D a rigid transformation can be written as

$$\begin{pmatrix} y_1 \\ y_2 \\ 1 \end{pmatrix} = \begin{pmatrix} R_{11} & R_{12} & T_1 \\ R_{21} & R_{22} & T_2 \\ 0 & 0 & 1 \end{pmatrix} \begin{pmatrix} x_1 \\ x_2 \\ 1 \end{pmatrix}, \tag{36}$$

where R_{ij} are elements in the rotation matrix

$$R = \begin{pmatrix} \cos\theta & -\sin\theta \\ \sin\theta & \cos\theta \end{pmatrix}. \tag{37}$$

The rotation matrix rotates the coordinates an angle θ around the origo. The matrix elements T_{ij} determines the translation of the coordinates. An general affine translation is described by the matrix

$$\begin{pmatrix} a_{11} & a_{12} & a_{13} \\ a_{21} & a_{22} & a_{23} \\ 0 & 0 & 1 \end{pmatrix} \tag{38}$$

This enables shear and scaling of the image.

If we apply a transformation matrix to an image, we get the new pixel coordinates of transformed image, but these points will not be on the grid coordinates of the image. For that reason, an interpolation scheme is applied to the transformed image coordinates to get the new pixel values at the grid coordinates. A suitable interpolation scheme must be chosen according to the given problem.

Image transformation can be divided into linear and non-linear transformation. For a linear transformation the same transformation matrix is applied to the whole image, whereas this is not the case for a non-linear transformation. Linear transformation is computationally faster and simpler, and less affected by noise. On the other hand, non-linear transformations can correct for local deformations out of reach for the linear transformation.

The difficult part of image registration is not to apply the transformation, but to obtain the right transformation matrix. The simplest case is the point or feature based method, where easily recognized feature are localized in both the fixed and moving image, either by interaction from the user, or by using a feature detection algorithm. In the case of an affine transformation, six pair of corresponding coordinates are needed to solve the set of linear equations to obtain the the six unknown elements in the transformation matrix. Usually, more points are obtained, and the transformation matrix is calculated using a least-squares approach.

5.3.2 Similarity measure

There are several ways of measuring the similarity between two images, where different approaches enhance different image properties, and are suitable for different problems. The choice of similarity measure will determine the minimum and the rate of convergence for the optimization scheme.

When the images to compare are from the same modality, they will be in the same intensity range. They will only differ because of noise, geometric transformation and changes in imaged object. Common similarity measures are then the sum of squared differences (SSD), the sum of absolute differences or the cross correlation. If the changes in the imaged object is sufficiently small, and we assume the noise to be Gaussian, it is shown in [24] that SSD give the optimal result. For two images A and B the SSD is given as

$$\text{SSD} = \sum_{i}^{N} |*|\, A_i - {B_i}^2, \forall i \in A \cap B, \tag{39}$$

where i is an image pixel. A closely related similarity measure is the Mean square error, $MSE = {}^{SSD}/_{N}$.

In multimodal image registration, the images have neither similar intensities or even a linear relationship between the intensities. For this type of problems, mutual information is the most common similarity measure. Mutual information is a measure of the statistical dependence of the two images, and the alignment is optimal the moving image contains the maximal amount of information about the fixed image. For a detailed review of mutual information in medical multimodal imaging, see [16].

5.3.3 Regular step gradient descent

An optimization scheme determines the optimal alignment by optimizing the chosen similarity measure. The optimization scheme is usually chosen through an empirical approach, where computational demand, reliability and stability are important factors.

The gradient descent method is a first-order algorithm which finds the local minimum of a multivarible, differentiable function $F(x)$. From a given initial state x_k, the optimizer moves a distance γ in the direction opposite to the gradient, i.e.

$$x_{k+1} = x_k - \gamma \Delta F(x_k). \tag{40}$$

This method suffers from the reliability of the step distance γ. Too long or short step will give a slow, or no convergence. The *regular step gradient descent* is a variation where the step length is halved every time there is a significant change in the direction of the gradient. The optimization terminates after reaching a the minimum, at a minimum step length, or after a maximum number of iterations.

To speed up the image registration, a pyramidal method can be applied together with the gradient descent. A smoothing filter is applied to the images, before they are decimated by a factor 2. This is performed for a given number of pyramid levels, resulting in a set of images with decreasing size. The scheme starts by optimizing the translation for the smallest image, and the optimal translation is used as an initial translation in the next pyramid level. In addition the increased speed, there is also less chance of getting stuck in a local minimum due to the smoothing which is applied before each decimation.

5.3.4 Interpolation

Interpolation is a mathematical method for obtaining new data points within the range of the current data points. Several different methods are common, all with a trade-off between performance and computational effort. For image interpolation nearest neighbor, bilinear and bicubic are most common, basic interpolation schemes. Nearest neighbor assign a value to the new data point equal the value of the nearest existing data point. The assigned value in bilinear interpolation is a linearly weighted sum of the closest existing data points with respect to the distance to the new data point.

For bicubic interpolation a cubic polynomial is calculated from the existing data to estimate the value at the new data point. This scheme is slower than nearest neighbor and bilinear, but the result is in general more smooth.

5.4 Background subtraction

Background subtraction is a method for visualizing the contrast agent in the ultrasound images. A background image is created from a set of images recorded before presence of contrast agent. The background is constructed by taking the maximum value of the chosen set at each pixel. The contrast agent can then be segmented from the image by subtracting the background image.

To ensure sufficient subtraction the background can be filtered before subtraction with a maximum filter. A maximum filter is a morphological filter which consider the neighborhood around a given pixel. The assigned value is equal the maximum value of the neighbors, and the size of the neighborhood is given by the size of the filter. In other words

$$B_{ij} = max(A_{kl}) \forall A_{kl} \in N, \tag{41}$$

where N is the neighborhood of A_{ij}, where A and B is the original and filtered image, respectively.

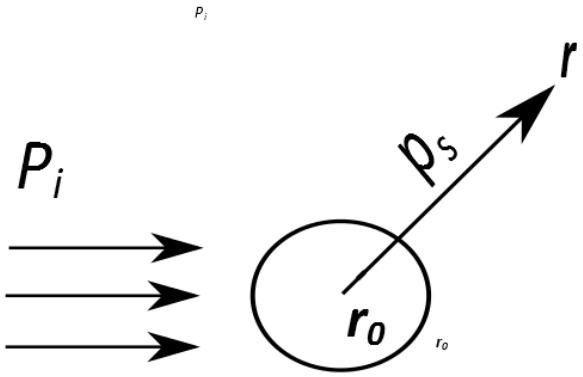

Figure 1: Fig:Scattering

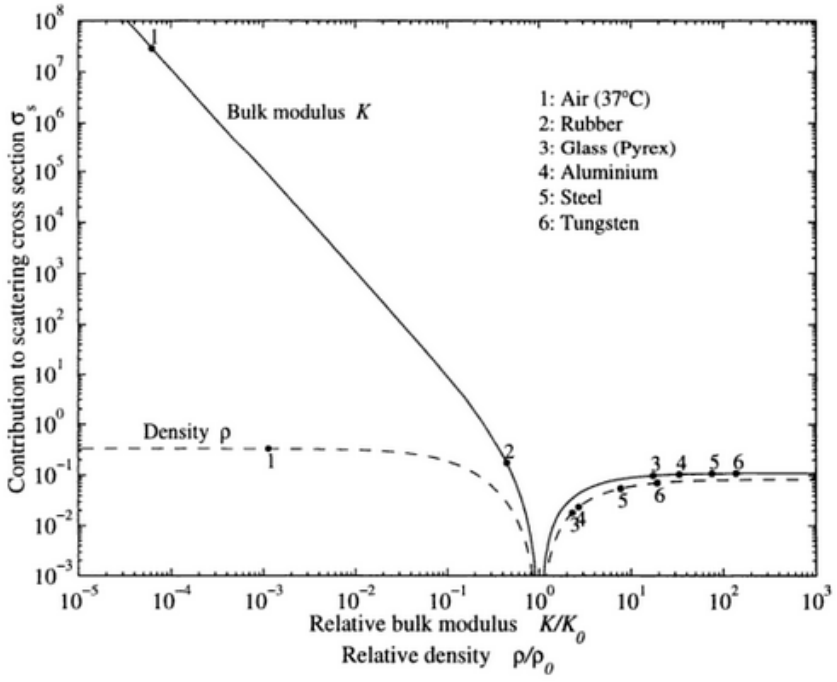

Figure 2: Contribution to Rayleigh scattering cross section from compressibility and density [**?**].

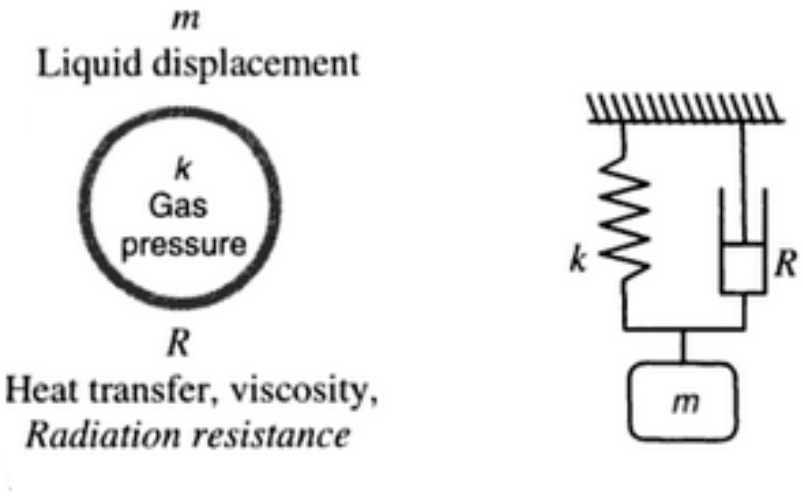

Figure 3: The bubble as a harmonic oscillator. Compared to the mass/spring system [**?**].

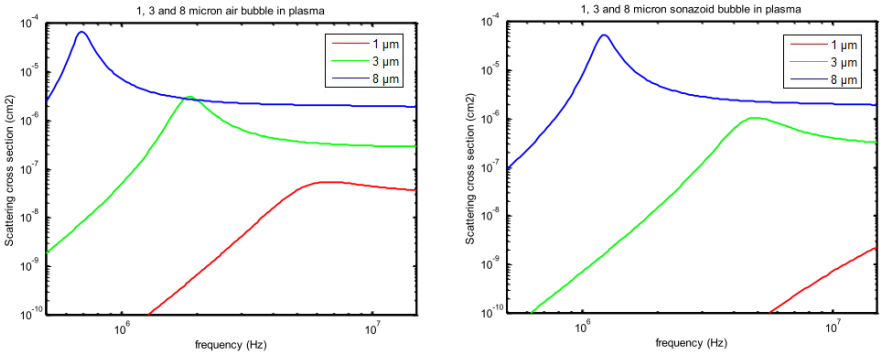

Figure 4: Left: Log-log plot of the scattering cross section σ_S for air bubbles with diameter 1, 3 and 8 µm. Right: Corresponding plot of Sonazoid™bubbles.

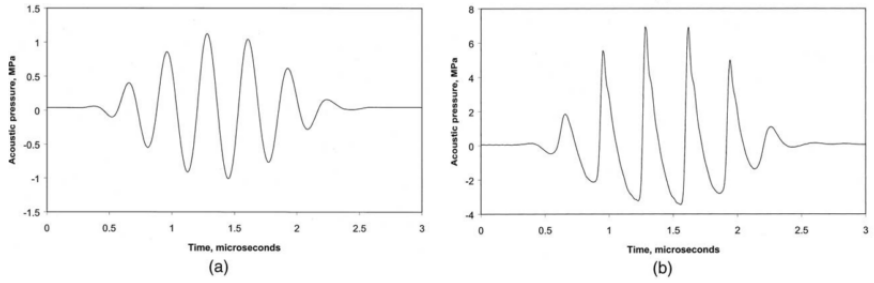

Figure 5: The measured focal waveform of a 3 MHz Doppler pulse in water for low acoustic pressure (a) and a pulse where the pressure is increased by 24 dB. The distortion of the waveform is easily seen in b [**?**].

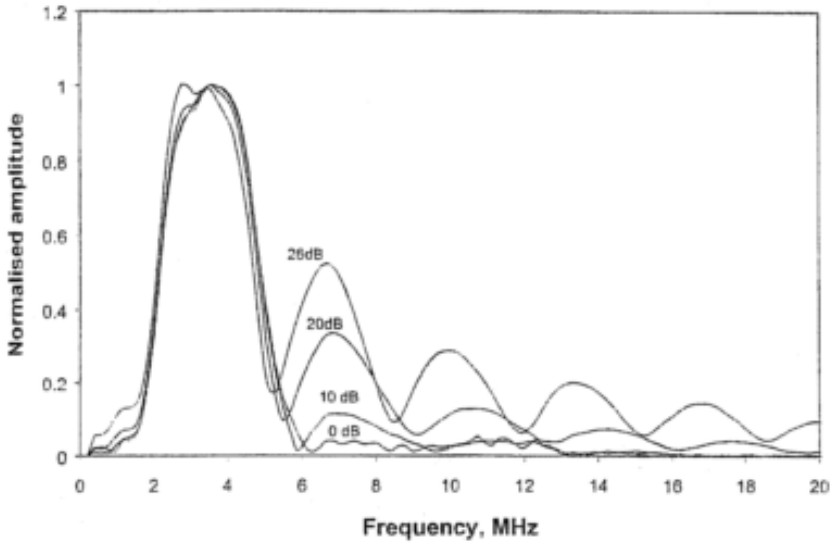

Figure 6: Development of harmonic frequencies as the amplitude of the source is increased by 10, 20 and 26 dB from a near-linear situation. Measured at the focus of a 3.5 MHz wave [?].

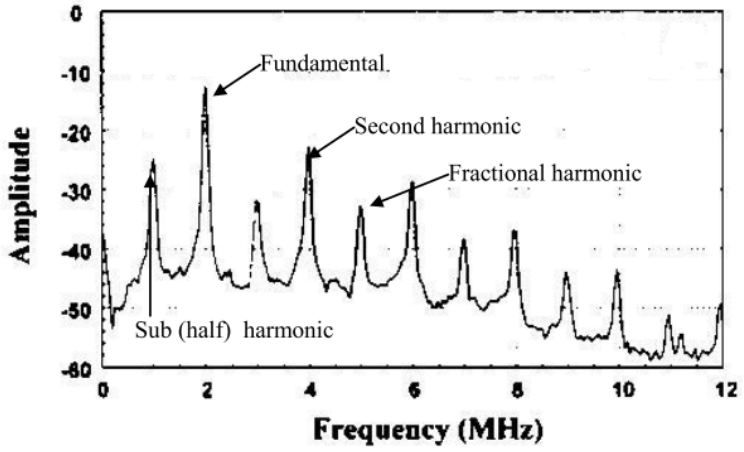

Figure 7: Spectrum of scattered signal from an Optison™microbubble, exposed to a signal with a fundamental frequency of 2 MHz. The other peaks are due to the non-linear response of the bubble [?].

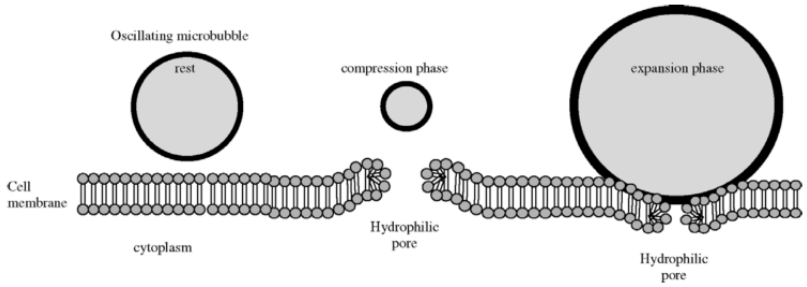

Figure 8: The oscillation moves the cell membrane and create hydrophilic pores which enables transport of fluid or macromulecules through the membrane [**?**].

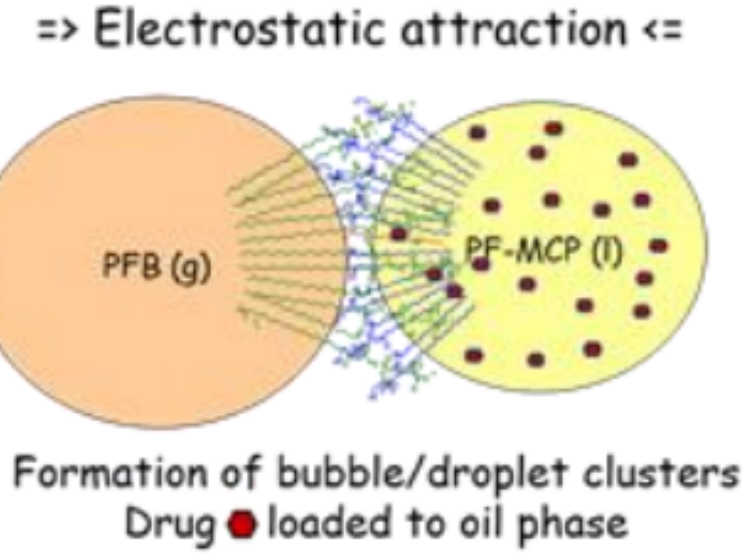

Figure 9: Illustration of phase-shift bubble, with the gas microbubble(left) and microdroplet(right).

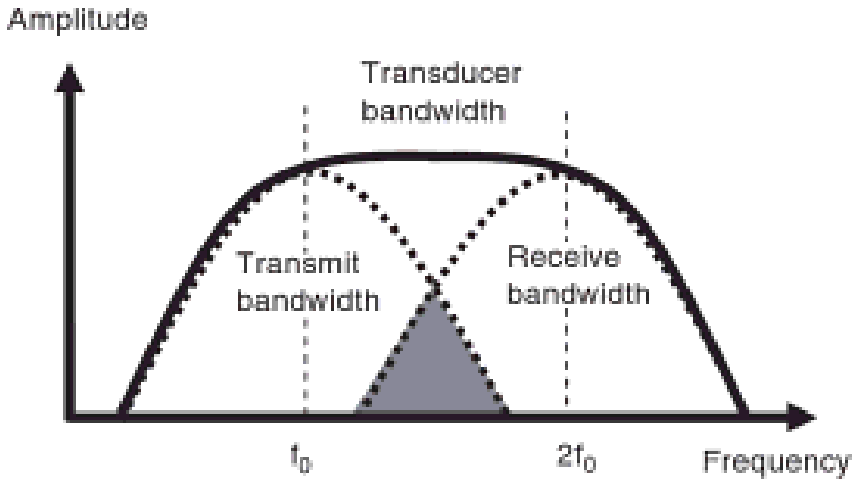

Figure 10: The transducer used in second harmonic imaging. The bandwidth cover both the fundamental frequency f_0 and the second harmonic $2f_0$ [**?**].

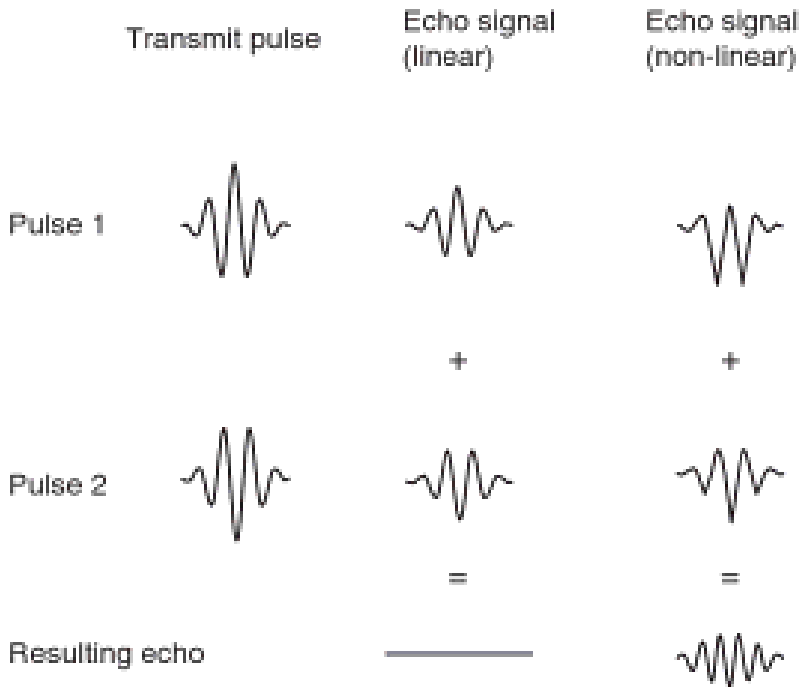

Figure 11: The two signal pulses used in phase-inversion are 180° out of phase. The non-linear signal is obtained from the sum of the two received signals [**?**].

6 Image recording

6.1 Sonazoid™

Sonazoid™is a contrast agent which has overcome all requirements stated in Section **??**, with a structure and size distribution as seen in Figure **??**. There is a core of perfluorcarbon gas, with a 4 nm thick lipid monolayer shell with shear modulus and viscosity equal (50 ± 3) MPa and $(0.8 \pm 0.1)\,\mathrm{N\,s\,m^{-2}}$, respectively [**?**]. The density of the perfluorcarbon gas core is $0.0098\,\mathrm{g\,cm^{-2}}$, while the thermal diffusivity is $0.07\,\mathrm{cm^2\,s^{-1}}$ [8].

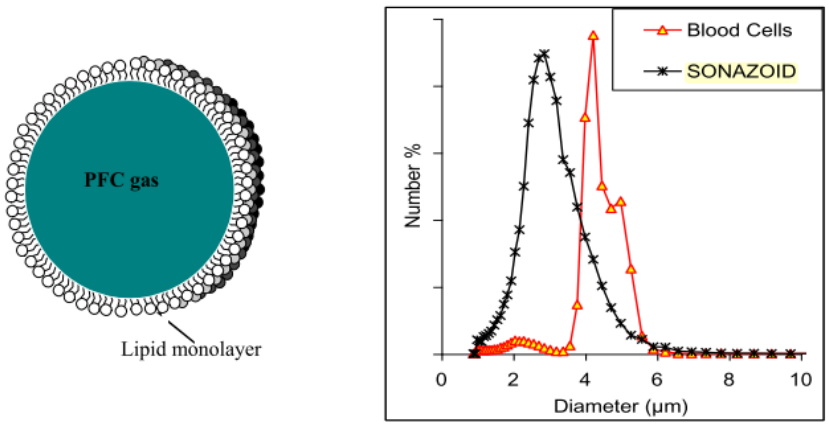

Figure 12: Left: The structure of Sonazoid™, i.e. perfluorcarbon gas encapsulated in a lipid monolayer. Right: Size distribution of Sonazoid™and red blood cells [8].

Sonazoid™microbubbles has been used together with microdroplets to form the ACT™clusters, or by itself in the test data sets. The microbubbles are shipped freeze-dried, and reconstituted with sterile water to crate a solution with a gas volume content of about 1%.

6.2 Imaging setup

All ultrasound images used in this research has been imaged with the Vevo®2100 imaging system from Visual Sonics. The imaging settings are presented in Table

6.2.1 Imaging modes

Two different imaging modes have been used, linear and non-linear contrast mode. Linear contrast mode has been used to visualize the ACT bubbles, while non-linear mode B-mode is used when only Sonazoid™is administered.

6.3 The animals/cancer

6.4 Counting 16 animals

For 16 animals, similar series of images have been captured, and phase-shift bubbles have been counted manually [**?**]. The same video sequences have been counted automatically to compare results.

7 Image processing

Image processing is performed on the acquired RF-data to enable image registration, background subtraction and counting of ACT microbubbles. The envelope of the RF-data from the absolute value of the IQ-modulated data. The RF-data are IQ-modulated through a Hilbert transform. A logarithmic compression is performed to reduce the dynamic range before image registration. The images are resized from $13568x256$ to $512x512$ through decimation and bicubic interpolation.

7.1 Image registration

Motion correction is performed on all videos. All frames are aligned to a reference frame through an affine transformation. A regular step gradient descent optimization scheme has been utilized to determine the transformation matrix. The maximum number of iterations in the optimization scheme was set to 2000, using only 1 pyramid level. The reference frame was constructed from an average of the three first frames of the video used for background subtraction.

7.2 Background subtraction

Before background subtraction the data is linearized. For each processed video a background is computed from a set of frames. The set of frames is chosen individually to minimize motion artifacts through a heuristic approach. The background is filtered with a maximum filter of size 3×3. The background is then subtracted from all frames to segment the signal caused by ACT™or Sonazoid™bubbles. Negative values after subtraction are set to 0.

7.3 Counting

The counting of ACT™bubbles are based on a temporal coherence filter to distinguish between stuck and free-flowing bubbles. A correlation matrix d of two

consecutive images ,A and B, is defined as

$$d_{ij} = 1 - \frac{|(|\, A_{ij} - B_{ij})}{A_{ij} + B_{ij}} \forall i, j. \tag{42}$$

A running average over correlation matrix for the last 40 frames is performed and indexes where the running average exceeds a temporal coherence threshold, d_{min} are considered stuck bubbles. The temporal coherence threshold is set to 0.85. This value is determined through a heuristic approach where the temporal coherence of manually identified bubbles are considered. A minimum intensity threshold is set to avoid counting of low-intensity noise. The minimum intensity threshold is set to 1000.

8 Qualitative validation

A qualitative validation of the counting algorithm was performed using the following approach. The counted video sequences was evaluated with the following prejudices. In video sequences with only Sonazoid™bubbles, no phase-shift bubbles should be counted. After the introduction of phase-shift bubbles the phase-shift bubbles should stick, and stay for up to five minutes before decaying and disappearing. After the burst of high-frequency ultrasound, all Sonazoid™bubbles should be destroyed, but none of the phase-shift bubble, i.e. the bubble count should not be affected by the high-frequency ultrasound.

9 Quantitative validation

9.1 Synthesized data set

A quantitative validation of the algorithm has been carried through by counting a synthesized data set with a known density of activated phase-shift bubbles. Video sequences of administration of Sonazoid™microbubbles were used as a background, and artificial phase-shift bubbles were added to the background to create a data set with a known number of phase-shift bubbles.

The algorithm for adding the phase-shift bubbles are now described. First, N random positions within the ROI is drawn from a uniform distribution. Then N intensities are drawn from a Gamma distribution, and N frame numbers are drawn from a Poisson distribution to determine when the bubbles enter the tumour. N bubbles are then generatedby applying the PSF to the drawn intensities. For each bubble the maximum intensity follows the slope of the bubble growth, shown in Figure **??**. These N bubbles are then log compressed and inserted into the video data.

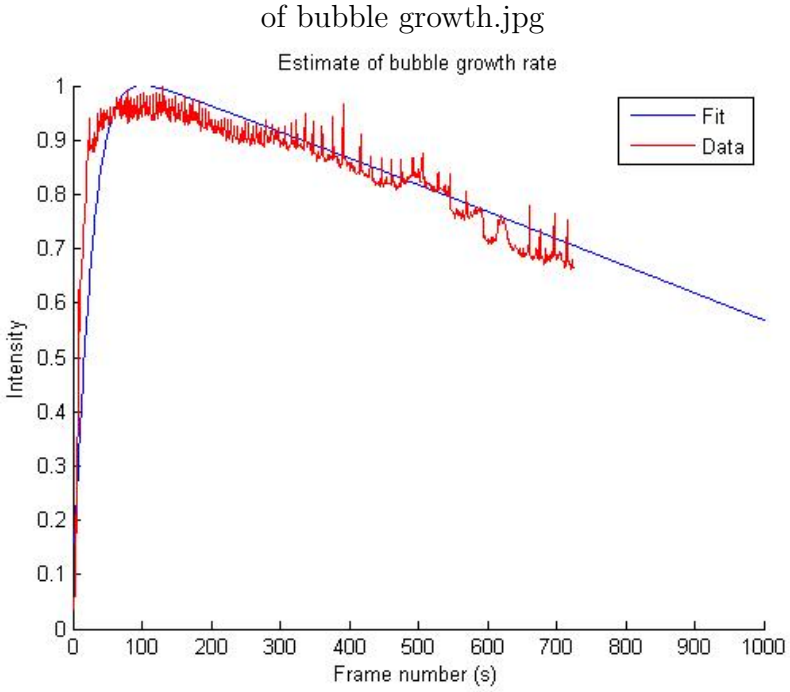

Figure 13: A growth slope is fit to data from an identified bubble in a true dataset.

9.2 Phase-shift bubbles intensity distribution

A heuristic approach was used to estimate the intensity distribution for the activated phase-shift bubbles. For a set containing 63 identified phase-shift bubbles the maximum intensity was plotted for each frame, see Figure **??**. For each bubble the overall maximum value was used in a set, from which a gamma distribution was estimated, see Figure **??**.

Measuring the point spread function

The point spread function was measured from two different images, image a low solution of Sonazoid™microbubbles in water and image of contamination in tap water. The size of the imaged microbubbles are smaller than the resolution of the imaging system, so the the bubbles seen in the image is effectively the point spread function(PSF). A two dimensional, normalized Gaussian function were fit to a single, easily identifiable bubble.

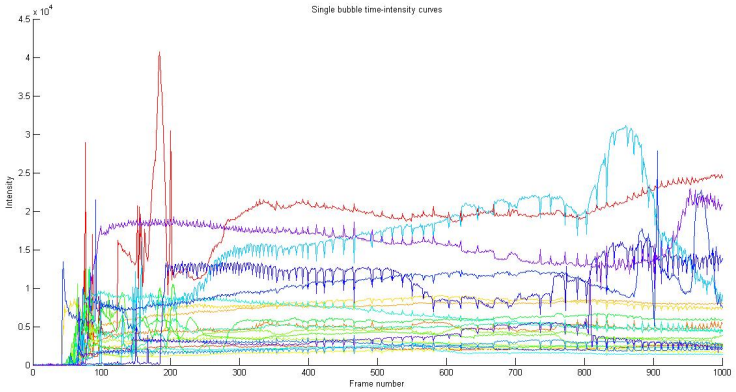

Figure 14: Time-intensity curves for a set of phase-shift bubbles.

Measuring the scan plane height

The height of the ultrasound scan plan is necessary for the estimate of the number of phase-shift bubbles per volume. This height was measured by imaging a thin wire, running diagonally across the scan plane. The image is then a mapping of the string down on the x-axis. The height, H, can the be calculated by measuring the length L, for a given angle Θ.

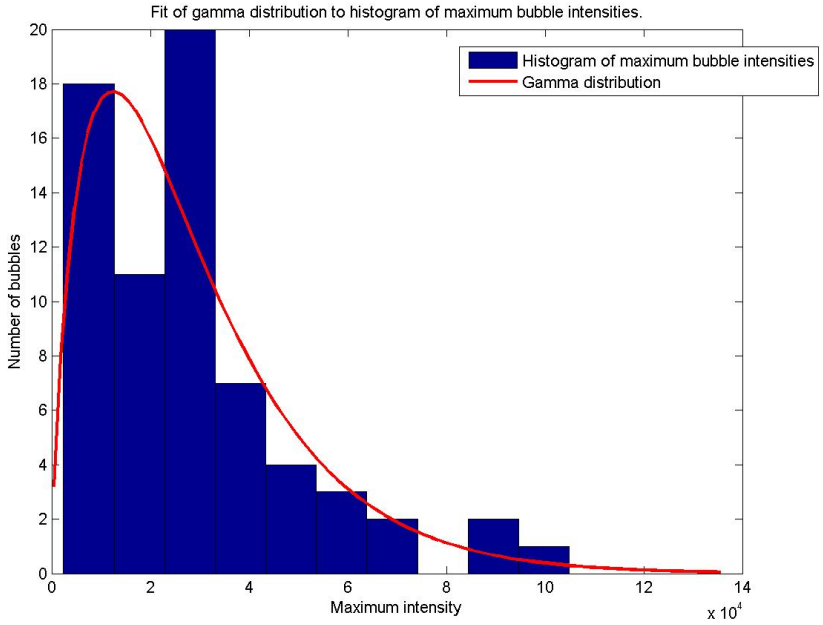

Figure 15: Fit of a Gamma distribution to the distribution of maximum phase-shift bubble intensities.

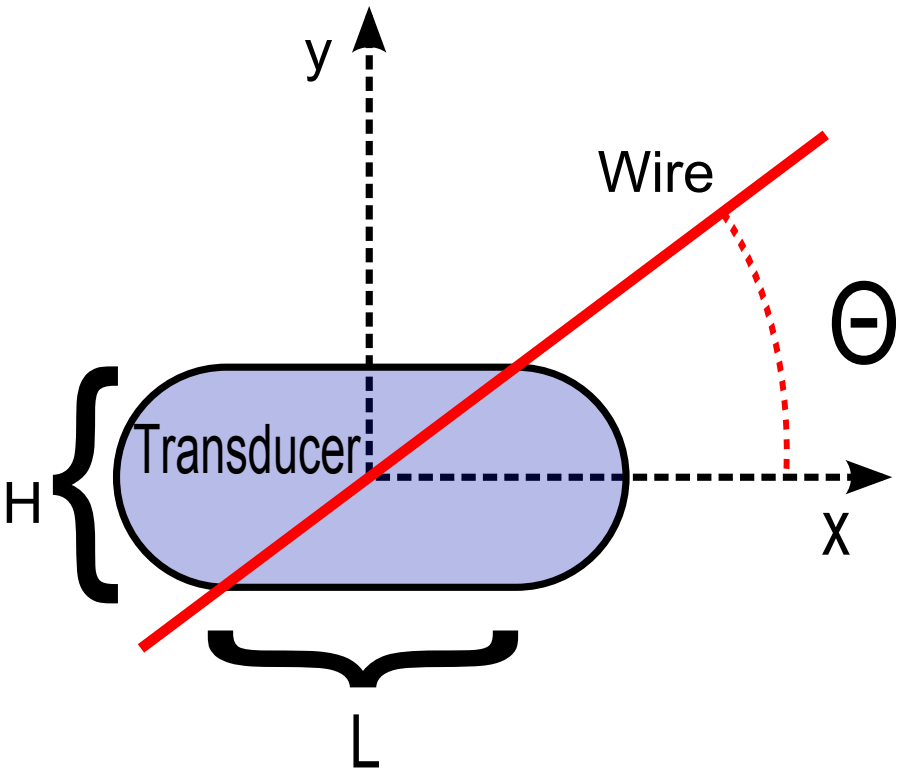

Figure 16: Measurement of transducer scan plane height

References

[1] David T Blackstock. *Fundamentals of physical acoustics*. John Wiley & Sons, 2000.

[2] Charles C Church. The effects of an elastic solid surface layer on the radial pulsations of gas bubbles. *The Journal of the Acoustical Society of America*, 97(3), 1995.

[3] Ronald E Crochiere and Lawrence R Rabiner. Interpolation and Decimation of Digital Signals-. 69(3):300–331, 1981.

[4] P A Dijkmans, L J M Juffermans, R J P Musters, A van Wamel, F J ten Cate, W van Gilst, C A Visser, N de Jong, and O Kamp. Microbubbles and ultrasound: from diagnosis to therapy. *European journal of echocardiography : the journal of the Working Group on Echocardiography of the European Society of Cardiology*, 5:245–256, 2004.

[5] Fitid Phase Equilibria, Elsevier Science Publishers B V, and Wright State Uniuersiry. The ostwald. 15:231–240, 1984.

[6] Maggie A Flower. *Webb's physics of medical imaging*. CRC Press, 2012.

[7] Andrew Healey. Batch PS0113 : Activated gas bubble size distribution dynamics via Sonometry system. 2013.

[8] Andrew Healey and P I Tx. Basic physical principles of medical ultrasound contrast agents. (August), 2012.

[9] Lars Hoff. *Acoustic characterization of contrast agents for medical ultrasound imaging*. Springer, 2001.

[10] Mousa Jafari, Bahram Zargar, and M Soltani. 15 Intelligent Drug Delivery Systems for Cancer Therapy.

[11] Virgil Craig Jordan. *Estrogen/antiestrogen action and breast cancer therapy*. Univ of Wisconsin Press, 1986.

[12] Roger John Benjamin King and Mike W Robins. *Cancer biology*. Pearson Education, 2006.

[13] Johan Kirkhorn. *Introduction to IQ-demodulation of RF-data*. IFBT, NTNU, 1999.

[14] Petros Koumoutsakos, Igor Pivkin, and Florian Milde. The Fluid Mechanics of Cancer and Its Therapy. *Annual Review of Fluid Mechanics*, 45(1):325–355, January 2013.

[15] T G Leighton. Derivation of the Rayleigh-Plesset equation in terms of volume. (308), 2007.

[16] F Maes, A Collignon, D Vandermeulen, G Marchal, and P Suetens. Multimodality image registration by maximization of mutual information. *Medical Imaging, IEEE Transactions on*, 16(2):187–198, April 1997.

[17] J B Antoine Maintz and Max A Viergever. A survey of medical image registration METHODS. 2(1):1–36, 1998.

[18] William C Moss. Rayleigh Plesset equation. 101(February 1997):1187–1190, 2014.

[19] Naoyo Nishida, Hirohisa Yano, Takashi Nishida, Toshiharu Kamura, and Masamichi Kojiro. Angiogenesis in cancer. *Vascular Health and Risk Management*, 2(3):213–219, August 2006.

[20] Charles L Shapiro and Abram Recht. Side Effects of Adjuvant Treatment of Breast Cancer. *New England Journal of Medicine*, 344(26):1997–2008, 2001.

[21] N.R. Soman, J.N. Marsh, M.S. Hughes, G.M. Lanza, and S.a. Wickline. Acoustic Activation of Targeted Liquid Perfluorocarbon Nanoparticles Does Not Compromise Endothelial Integrity. *IEEE Transactions on Nanobioscience*, 5(2):69–75, June 2006.

[22] Esra Talu, Kanaka Hettiarachchi, Shukui Zhao, Robert L Powell, Abraham P Lee, L Longo, and Paul A Dayton. Possible Method for Improving Sensitivity in Molecular Imaging. 6(6):384–392, 2008.

[23] E Glen Tickner and Cardiology Division. WHY DO THE LUNGS CLEAR ULTRASONIC CONTRAST ?*. 6, 1980.

[24] Paul Viola and William M Wells Iii. Alignment by Maximization of Mutual Information. 24(2):137–154, 1997.

[25] P N T Wells. *Physical principles of ultrasonic diagnosis*. Medical physics series. Academic Press, 1969.

A Derivation of the Rayleigh-Plesset equation

The Rayleigh-Plesset equation is an ordinary differential equation which describe the non-linear oscillation of a gas bubble suspended in an infinite liquid, subject to an external sound wave. This equation is in the following derived using the energy balance between the liquid and the gas bubble [18]. The equation can also be derived from the Navier-Stokes equations [15].

A few assumptions are required for the following derivation to be valid. We assume the wavelength of the pressure field to be way larger then the size of the gas bubble, i.e. $d \ll \lambda$. The bubble is spherical and spatially uniform conditions within the bubble exist at all times. We can neglect gravity and bulk viscosity. There is no flow of either matter of heat through the boundary of the bubble. The density of the gas is significantly smaller then the liquid density, and the gas within the bubble can be considered an ideal gas. Using these assumptions the oscillation will be an adiabatic process. Newton's notation for the time-derivative is used.

Consider an oscillating bubble suspended in incompressible fluid. Because of the incompressility of the fluid, the fluid velocity $u(r,t)$ has to follow the inverse square law, i.e.

$$(\mathbf{??})u(r,t) = \frac{R(t)^2}{r(t)^2}\dot{R}(t). \tag{43}$$

Here $R(t)$ is the bubble radius, $\dot{R}(t)$ the velocity of the boundary and r any radius larger or equal R.

The kinetic energy E_k of the fluid caused by the oscillating bubble is then

$$E_k = \frac{\rho_l}{2}\int_R^\infty u(r,t)4\pi r^2 dr = 2\pi\rho_l R^3\dot{R}^2, \tag{44}$$

where ρ_l is the liquid density.

Far from the bubble the liquid pressure is given by $p_\infty(t) = p_0 + p(t)$, where $p(t) = p_a e^{i\omega t}$ is the time varying pressure caused by the sound wave and p_0 the hydrostatic pressure. For an adiabatic process we have that $pV^\gamma = \text{constant}$. Here V is the volume, p the pressure and γ the adiabatic index. The pressure is then only a function the radius R,

$$p(R) = p_{R_0}\left(\frac{V_{R_0}}{V(R)}\right)^\gamma = p_{R_0}\left(\frac{R_0}{R}\right)^{3\gamma}, \tag{45}$$

where R_0 and p_{R_0} are the equilibrium radius and pressure.

The work done to expand the bubble is only carried out by the net pressure, $\Delta p = P(R) - P_\infty(t)$, and the total work W is

$$W = \int \Delta p dV = \int_{R_0}^{R} (p(R) - p_{\infty(t)}) 4\pi R^2 dR. \tag{46}$$

The kinetic energy of the liquid must equal the work, and the Rayleigh-Plesset equation is obtained by equating and differentiating Equation (44) and Equation (46) with respect to R,

$$\frac{p_{R_0}\left(\frac{R_0}{R}\right)^{3\gamma} - p_0 - p(t)}{\rho_l} = \frac{3\dot{R}^2}{2} + R\ddot{R}. \tag{47}$$

Note that $\frac{d\dot{R}^2}{dR} = 2\ddot{R}$.